Journal of Catalysis 271 (2010) 88–98

Contents lists available at ScienceDirect

Journal of Catalysis

journal homepage: www.elsevier.com/locate/jcat

Tailoring the mesopore structure of HZSM-5 to control product distribution in the conversion of propanal

Xinli Zhu, Lance L. Lobban, Richard G. Mallinson, Daniel E. Resasco *

Center for Biomass Refining, School of Chemical, Biological, and Materials Engineering, The University of Oklahoma, Norman, OK 73019, USA

ARTICLE INFO

Article history:
Received 23 September 2009
Revised 14 December 2009
Accepted 2 February 2010
Available online 6 March 2010

Keywords:
Propanal
HZSM-5
Desilication
Biomass conversion
Bio-oil upgrading

ABSTRACT

Conversion of propanal to gasoline-range molecules was investigated over a series of HZSM-5 catalysts with controlled mesoporosity generated by desilication. Characterization of the structure of the solid by powder X-ray diffraction (XRD), scanning electronic microscopy (SEM), ammonia and isopropylamine temperature programmed desorption (TPD), and *n*-butane diffusivity measurements confirmed the development of various degrees of mesoporosity in the zeolites. This structural modification seems to have little influence on Brønsted acid density. The catalyst stability was improved upon desilication due to an increase in coke tolerance. The product distribution of the propanal conversion was found to vary with the severity of the desilication. Increasing the extent of desilication gradually reduced the aromatization and cracking reactions, due to a reduction in the fraction of micropores and in the diffusion path length. Mildly desilicated samples were found to exhibit the best stability on stream and inhibited coke formation.

1. Introduction

Conversion of lignocellulosic biomass into liquid hydrocarbon fuels provides a CO_2 neutral energy production route, which potentially can reduce the dependency on fossil fuels [1–3]. In the thermochemical route (e.g. fast pyrolysis), the molecular structure of biomass is broken down into smaller fragments that subsequently undergo further conversion in the vapor and liquid phases condensing into a complex product termed bio-oil. Some of the constituents of this product are larger than the desirable fuel range, others are shorter, but all of them contain significant amounts of oxygen. The chemically unstable, highly viscous, corrosive, and low-heating value liquid product includes acids, aldehydes, ketones, phenolic compounds, sugars, and dehydrosugars [4,5]. Deoxygenation of the larger oxygenated molecules (guaiacols, vanillins, cresols, catechol, etc.) is being extensively investigated [6–10]; and hydrogenation, hydrogenolysis, and decarbonylation are potential reaction pathways to improve the quality of these heavy molecules. By contrast, the short oxygenates (e.g., aldehydes, acids, ketones) need to be condensed into larger molecules to become useful fuel components. Under hydrotreating conditions for refining the complete bio-oil, short oxygenates are converted to light hydrocarbons of low value while consuming substantial hydrogen. Alternative strategies that avoid discarding short oxygenates should be considered since they constitute a significant fraction of the product [4,5]. Due to the highly complex nature of the bio-oil, understanding the reaction pathways for each kind of compound conversion is highly desirable for catalyst and process screening. Therefore, the study of model compounds is the first step in simplifying the complexity of the problem [11–14]. While our next studies will include more complex mixtures, in this work, propionaldehyde (propanal) has been selected as a model compound to investigate the conversion of short aldehydes into gasoline-range molecules.

The study of propanal conversion is also relevant to the utilization of glycerol, a major by-product of bio-diesel production. Glycerol is readily converted into acrolein by dehydration [15,16]. Subsequent hydrogenation produces propanal [17]. Thus, conversion of propanal may also represent a potential approach for the conversion of bio-diesel by-products to gasoline-range fuels.

Previous studies on the conversion of small oxygenates (methanol, ethanol, etc.) to hydrocarbons (alkene/alkane, aromatics) over zeolites have addressed propanal conversion briefly. It has been reported that propanal can yield aromatics in higher selectivity than acetone and much higher than other C_3 oxygenates (alcohol, acid, ester) [18–20]. However, it was also found that propanal causes a rapid catalyst deactivation [19].

Zeolites are widely used in hydrocarbon conversion due to their high density of strong acid sites and their well-defined microporous channel structure that enable shape selective reactions inside the pore channels. However, transport of both reactants and products in and out of the micropores may be limited by diffusion. Conventional mesoporous materials such as MCM-41 and SBA-15 have superior diffusion properties but lower thermal/hydrothermal

* Corresponding author. Fax: +1 405 325 5813.
E-mail addresses: mallinson@ou.edu (R.G. Mallinson), resasco@ou.edu (D.E. Resasco).

0021-9517/$ - see front matter © 2010 Elsevier Inc. All rights reserved.
doi:10.1016/j.jcat.2010.02.004

stability and weaker acidity. To improve the performance of zeolites by enhancing transport, a post-synthesis method called desilication has been used [21–25]. This method selectively removes silica from the zeolite crystals, generating mesopores. The resultant material has a hierarchical pore structure with pores of varying dimensions and with a shortened diffusion path length for reactants and products [26,27], as well as improved accessibility for large molecules [28–30]. Desilicated zeolites have been investigated in several reactions, including cumene cracking, methanol to propylene, methanol to gasoline, hydroxylation of benzene to phenol, methane aromatization, and hexene conversion [29–35]. In most cases, improved activity, stability, and selectivity have been reported. In general, the observed improvement has been ascribed to enhanced diffusion due to the generation of mesopore channels. In this work, four zeolite samples with varying degree of desilication have been characterized for changes in texture, structure, acidity, and diffusivity, and then used in the conversion of propanal with the objective of investigating the effects of mesopore generation on the conversion and selectivity toward gasoline-range products. H-ZSM-5 has been chosen as the basis for this study due to its well-known activity for the conversion of short oxygenates to aromatics.

2. Experimental

2.1. Zeolite synthesis and desilication

The parent zeolite was synthesized hydrothermally using sodium aluminate (Aldrich) dissolved in deionized water as the Al source to which tetrapropylammonium hydroxide (Fluka, 20% TPAOH) was first added under stirring as the structure directing agent, silica gel (Ludox, 40%) was then added dropwise while stirring, as the Si source. The resultant gel composition was $150SiO_2{:}1.0Al_2O_3{:}8TPAOH{:}1600H_2O$ (Si/Al = 75). After stirring at 700 rpm for 10 h at room temperature, the gel was transferred to a Teflon-lined autoclave, where the zeolite crystallized at 180 °C over 5 days with stirring at 60 rpm. The solid product was recovered by filtration, washed, dried at 110 °C, and finally calcined in air at 550 °C for 6 h to remove the template.

Four desilicated samples (*DS1*, *DS2*, *DS3*, and *DS4*) were prepared by varying the basicity of the alkaline solution, treatment temperature, and time, resulting in different extents of silica removal. To achieve the desired level of desilication, the parent sample (*P*) was treated in the following desilication baths, keeping in all cases a ratio of 30 mL solution per gram of zeolite and using 350 rpm stirring rate. *DS1*: 0.45 M Na_2CO_3 (Aldrich) solution for 30 h at 75 °C; *DS2*: 0.2 M NaOH (Aldrich) solution at 65 °C for 30 min; *DS3*: at 80 °C for 30 min, and *DS4*: at 80 °C for 4 h. After each treatment, the desilication was stopped by quenching the sample in an ice-water bath. The resultant samples were then filtered, washed, and dried at 110 °C overnight. After this step, the samples were further suspended in deionized water at 80 °C for 2 h to remove any amorphous silica and alkaline metals remaining in the solid. Finally, the samples were again filtered, washed, and dried at 100 °C overnight.

The H-form of the zeolite was obtained by repeating three times the ion exchange of the Na-form of the zeolite with 1 M NH_4NO_3 (Aldrich) solution (10 mL/g) at 80 °C for 10 h. After each exchange, the samples were filtered, washed, and dried, and finally calcined in flowing air at 550 °C for 4 h.

2.2. Catalyst characterization

Powder X-ray diffraction (XRD) patterns of the zeolite samples were recorded using a Bruker D8 Discover diffractometer, with a Cu Kα radiation source (λ = 1.54056 Å). High resolution scanning electronic microscopy (SEM) observations were performed on gold-coated samples in a Jeol JSM-880 electron microscope equipped with X-ray elemental analyzer. Nitrogen adsorption measurements [36] were performed in an Autosorb-1 analyzer (Quantachrome) at liquid nitrogen temperature after outgassing the samples under vacuum at 300 °C for 5 h. The micropore volume (V_{micro}) and micropore surface area (S_{micro}) were derived by the *t*-plot method [37] using the adsorption data of $0.2 < p/p_0 < 0.6$. The mesopore size distribution was obtained from the BJH method [38] applied to adsorption branch [39] data for $p/p_0 > 0.35$. Finally, the total pore volume was determined at $p/p_0 = 0.99$.

The acid properties of the various zeolites were characterized by temperature programmed desorption of ammonia (NH_3-TPD) and isopropylamine (IPA-TPD), using a 0.25 in. o.d. quartz reactor. Before each experiment, the zeolite sample (100 mg for NH_3-TPD and 50 mg for IPA-TPD) was pretreated for 0.5 h in flowing He (30 mL/min) at 600 °C to eliminate any adsorbed water. Then, the temperature was reduced to 100 °C, and the sample was exposed to NH_3 (2% NH_3/He, 30 mL/min, 30 min) or to IPA (4 μL/pulse, 10 pulses, 3 min/pulse). After exposure to the respective adsorbate, He flowed for 0.5 h to remove weakly adsorbed NH_3 or IPA. To start the TPD, the temperature was increased to 650 °C at a heating rate of 10 °C/min. The evolution of desorbed species was continuously monitored by a Cirrus mass spectrometer (MKS) recording the following signals m/z = 17 and 16 (NH_3), 18 (H_2O), 44 (IPA), and 41 (propylene). The density of acid sites was quantified by calibrating the MS signals using the average of 10 5-mL-pulses of 2% NH_3/He.

The changes in diffusivity upon desilication were evaluated by sending an *n*-butane pulse using the same system used for TPD. The zeolite samples (100 mg, 40–60 mesh) were pretreated in flowing He (30 mL/min) at 400 °C for 0.5 h to remove water. Then, the temperature was reduced to 90 °C, and a 5 mL *n*-butane pulse (10% *n*-butane/He) was sent under flowing He (30 mL/min). The butane concentration was monitored by following the m/z = 43 signal in a mass spectrometer (MS) and compared to pulses over nonporous blanks.

The amounts of coke deposits were quantified by Temperature Programmed Oxidation (TPO) by passing a 2% O_2/He stream over a 20 mg spent catalyst sample, using a linear heating rate of 10 °C/min. The signals of H_2O (m/z = 18), CO_2 (m/z = 44), and CO (m/z = 28) were continuously monitored by MS. Quantification was calibrated on the basis of the signals from 100 μL CO_2 and CO pulses in flowing He.

2.3. Catalytic measurements

The catalytic performance of the different samples was examined in a quartz reactor (1/4 in. o.d.) at atmospheric pressure. The catalyst sample (10–400 mg, 40–60 mesh) was packed in the reactor between two layers of quartz wool. The thermocouple was affixed to the external wall of the reactor close to the catalyst bed. The temperature of the catalyst bed was increased to 400 °C using a rate of 10 °C/min and held at 400 °C for 0.5 h in flowing H_2 (35 mL/min) before reaction. Liquid propanal (from Aldrich) was fed using a syringe pump (kd scientific) equipped with a needle at a rate of 0.12 mL/min. The liquid was completely vaporized in the line before entering the reactor. All lines were kept at 300 °C to avoid condensation of reactant or products. The products were analyzed online using a gas chromatograph (GC 6890, Agilent) equipped with a flame ionization detector (FID) and a 60 m Innowax capillary column. The effluent was trapped in methanol using an ice-water bath and analyzed using a QP2010s GC–MS (Shimadzu) with an Innowax column. Quantification of products was done by combination of GC–MS analysis and injection of known amounts of standard compounds. The space time (W/F) is defined

as the ratio of catalyst mass (g) to propanal mass flow rate (g/h) with a carrier gas flow rate of 30 mL/min. The range of W/F used in this study was 0.1–4.0 h. The propanal conversion and product yield were calculated based on carbon atoms.

3. Results

3.1. Catalyst characterization of desilicated samples

3.1.1. Porous structure

As shown in Table 1, different levels of desilication were obtained by treating the ZSM-5 zeolite with various solutions that ranged from a weakly basic solution (Na_2CO_3) to a strongly basic solution (NaOH) that is very effective in removing silica species from the zeolite crystal even at low temperatures and short times. As a result, the weight loss gradually increased from *DS1* (22%) to *DS4* (52%) as the severity of the treatment increased. It has been suggested that negatively charged AlO_4^- protects against OH^- attack, whereas the Si—O—Si bond is more easily attacked by OH^- [21–25]. In agreement with previous studies, the calculated Si/Al ratios that result from assuming that only silica is removed are consistent with the elemental analysis data obtained in the SEM by EDX.

Fig. 1 shows that even though a significant amount of silica was removed from the zeolite, the XRD patterns show that the MFI structure is preserved. However, a close examination of the characteristic peaks of MFI structure in the 2θ range of 23–25° (see the inset in Fig. 1), revealed a slight shift in the peak positions to lower angles for the desilicated samples. This shift may be interpreted as a slight expansion of the unit cell of the zeolites, which could be ascribed to the selective removal of Si. This result is in agreement with those of Ohayon et al. [40], who reported that the micropores were slightly enlarged by the desilication-stabilization process. It must be noted that in the most heavily desilicated sample (*DS4*), the diffraction peaks appear to shift back to higher angles. This reversed structural modification could be explained by a previously reported 'healing effect' [22,33] undergone by the zeolite after prolonged treatment that allows some of the dissolved Si species to re-insert back into the zeolite framework.

The SEM micrographs of the parent sample (*P*) show well-crystallized particles of ~6 μm (Fig. 2a). The particles are twinned crystals (Fig. 2b), and the well-defined surfaces are rather smooth with few defects (Fig. 2c). Desilication seems to break up some of the particles into smaller fragments (Fig. 2d). The surface becomes rougher even for those particles that preserve their original shape and size (Fig. 2e). The higher-magnification image (Fig. 2f) shows evidence of the presence of etched channels on the surface of the particle, indicating the development of mesoporosity.

Fig. 3a and b shows the N_2 adsorption–desorption isotherms and the results of the BJH analysis for both the parent and desilicated HZSM-5 samples. The increased adsorption in the range $p/p_0 > 0.5$ and the appearance of hysteresis loops in the desorption branch

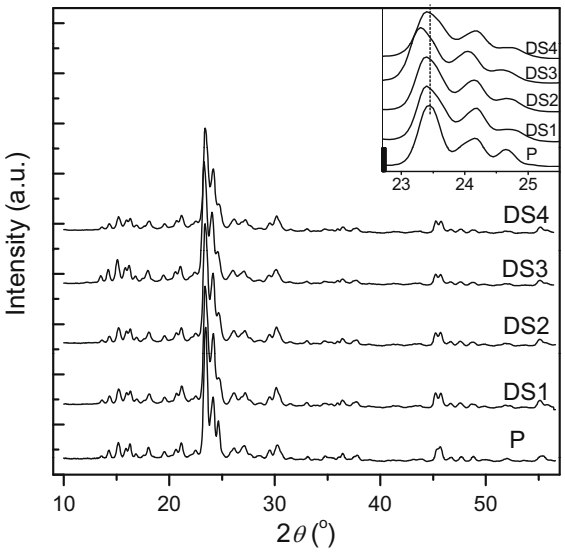

Fig. 1. XRD patterns of parent zeolite (*P*) and desilicated HZSM-5 samples (*DS1* to *DS4*) of increasing desilication severity.

at p/p_0 of ~0.42 of the desilicated samples indicate the development of mesopores. From the analysis of the data, it can be inferred that the treatment in weak base (Na_2CO_3) for prolonged times (*DS1*) results in a relatively wide distribution of pore sizes, centered at 12.0 nm but with a rather small overall pore volume. By contrast, the treatment with the strong base (NaOH) at low temperatures (sample *DS2*) results in a relatively narrower pore size distribution centered at 7.3 nm and a larger overall pore volume. Increasing the severity of the NaOH treatment by using higher temperatures and longer times (*DS3* and *DS4*), results in a gradual increase in both pore size and overall pore volume, with a peak center at 10.7 and 13.9 nm, respectively. The results from the N_2 adsorption are summarized in Table 1. They confirm that the fraction of mesoporosity significantly increases at the expense of the microporosity with increasing desilication severity. The results of the effect of temperature and time of alkaline treatment are in good agreement with those reported by Groen et al. [25,39,41]. It is noted that the V_{micro} is slightly increased for *DS1*, possibly as a result of the prolonged treatment time with the weakly basic Na_2CO_3. This long treatment may lead not only to the removal of Si but also to re-incorporation of some of the dissolved species into the zeolite structure, further creating microporosity.

3.1.2. Acidity

The effects of desilication on the acidity of the HZSM-5 zeolites were studied by TPD of adsorbed NH_3 and IPA, as shown in Figs. 4 and 5, respectively. For sample *P*, two distinct desorption peaks are observed at 180 °C and 385 °C in the NH_3-TPD. These are usually ascribed to NH_3 desorption from weak and strong acid sites,

Table 1
Weight loss, final Si/Al ratio, specific area (S_{BET}), and pore volume of parent (*P*) and desilicated (DS) zeolite samples.

Sample	W_{loss} (wt.%)	Si/Al[a]	Si/Al[b]	S_{BET} (m^2/g)	V_{total} (cm^3/g)	V_{micro} (cm^3/g)	V_{meso}[c] (cm^3/g)	S_{micro} (m^2/g)	S_{meso}[c] (m^2/g)	V_{meso}/V_{micro}
P	–	–	76	392	0.217	0.161	0.056	359	33	0.35
DS1	22	59	62	414	0.297	0.171	0.126	369	49	0.74
DS2	28	54	52	429	0.352	0.151	0.201	335	94	1.33
DS3	48	39	42	453	0.433	0.138	0.296	310	143	2.14
DS4	52	36	37	441	0.492	0.138	0.354	311	130	2.56

[a] Estimated from weight loss (W_{loss}) assuming that only silica was removed.
[b] Estimated by SEM elemental analysis of several particles.
[c] $V_{meso} = V_{total} - V_{micro}$, $S_{meso} = S_{BET} - S_{micro}$.

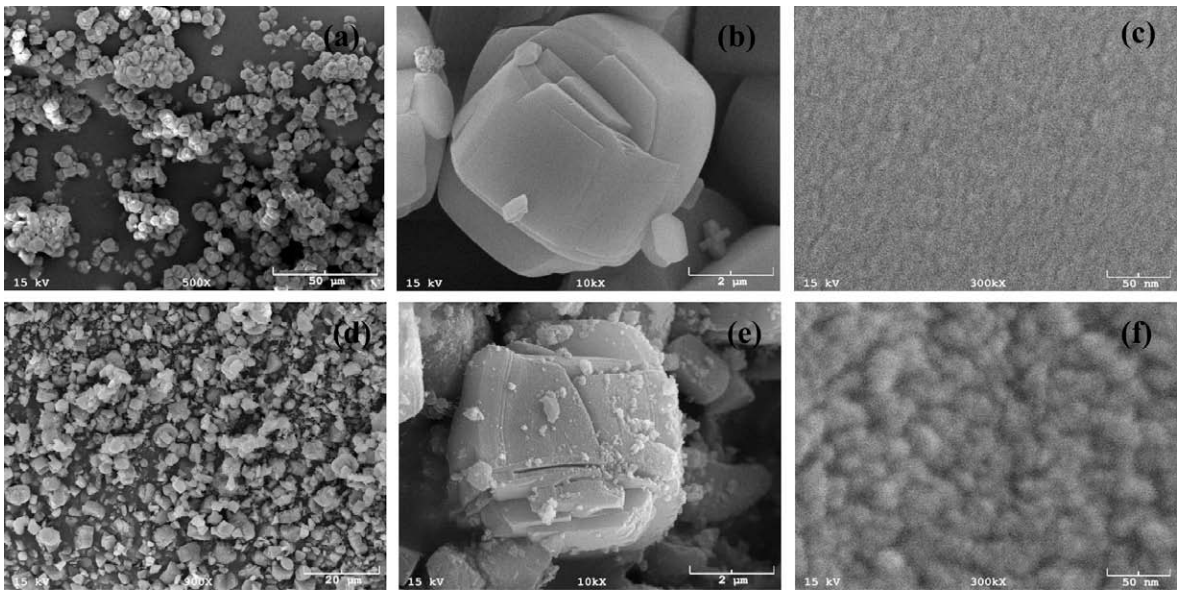

Fig. 2. SEM micrographs of parent zeolite sample *P* (a–c) and desilicated sample *DS2* (d–f).

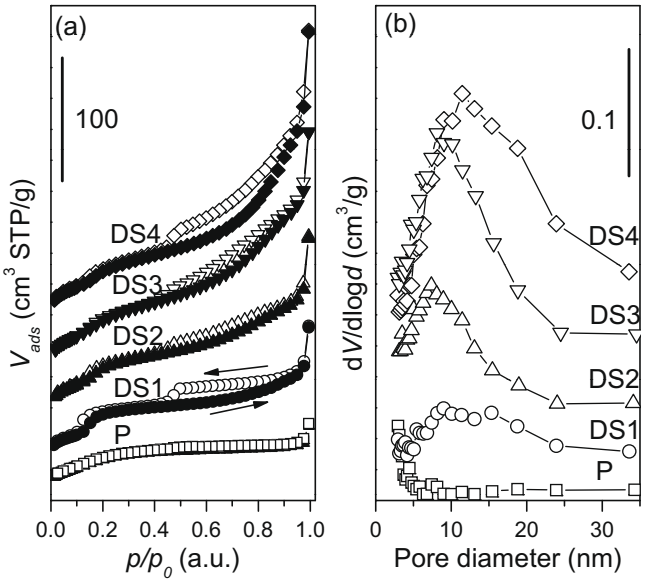

Fig. 3. N_2 adsorption–desorption isotherms (a) and mesopore pore size distributions (b) of parent zeolite (*P*) and desilicated zeolite samples (*DS1* to *DS4*) of increasing desilication severity.

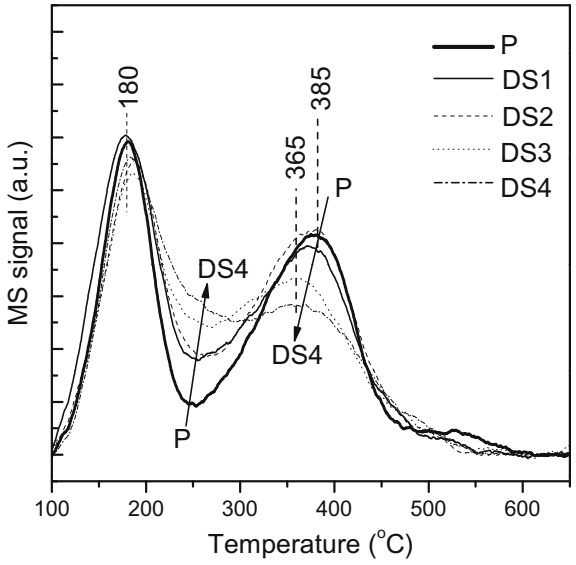

Fig. 4. NH_3-TPD profiles of parent zeolite (*P*) and desilicated zeolite samples (*DS1* to *DS4*) of increasing desilication severity.

respectively. With increasing desilication severity from *DS1* to *DS4*, it is observed that the peak ascribed to strong acid sites gradually loses its intensity and shifts to lower temperatures. These changes are accompanied by a gradual increase in the intensity at intermediate temperatures (~250 °C), but little change in the peak ascribed to weak acid sites. These changes either indicate that desilication converts some of the strong Brønsted acid sites into sites of weaker acidity or modifies the accessibility of these sites due to the partial removal of silica.

The advantage of the IPA-TPD method is that it can be used to selectively quantify Brønsted acid sites that catalyze the conversion of IPA into propylene and NH_3 [42–45]. For the undissociated IPA (Fig. 5a), upon desilication, the intensity of the peak at ~190 °C becomes smaller than that for the parent sample; at the same time, a small peak at higher temperatures (~250 °C) gradually develops with increasing desilication severity. The former peak could be ascribed to desorption of the undissociated amine from weak acid sites of Si—OH. The reduction in intensity is probably due to the removal of internal Si—OH sites (silanol nests, i.e. surface defects). This explanation is in good agreement with previous IR measurements that showed that internal Si—OH sites were removed upon desilication [25,33,46]. A new peak develops at higher temperatures with increasing desilication severity. Desorption from these sites occurs at relatively high desorption temperatures, but they are unable to catalyze the IPA decomposition [42–45]. Infrared measurements of pyridine adsorption have shown an increase in the density of Lewis acid sites due to dealumination upon severe desilication [29,31,46]. Accordingly, this desorption peak may be associated with the presence of those sites. In all samples, the Brønsted sites produced propylene desorption peaks centered at 351 °C (Fig. 5b), indicating that the density (and possibly strength)

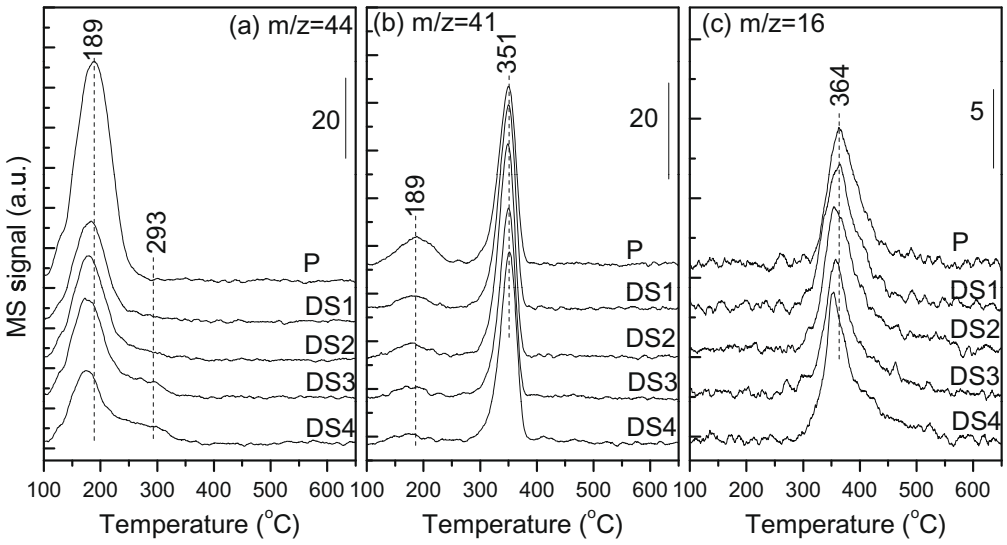

Fig. 5. TPD profiles of adsorbed isopropylamine on the parent zeolite (sample *P*) and desilicated zeolite samples (*DS1* to *DS4*) of increasing desilication severity.

Table 2
Total acid density (A_{total}) and Brønsted acid density (A_B).

Sample	*P*	*DS1*	*DS2*	*DS3*	*DS4*
A_{total} (mmol/g)	0.26	0.29	0.29	0.27	0.27
A_B (mmol/g)	0.20	0.23	0.24	0.22	0.22

A_{total} was derived from NH_3-TPD, and A_B was derived from and IPA-TPD.

Table 3
Apparent diffusivity (*D*) for *n*-butane.

Sample	*P*	*DS1*	*DS2*	*DS3*	*DS4*
D ($\times 10^{-10}$ m^2/s)	5.46	4.93	5.61	7.93	9.44

of Brønsted acid sites is not significantly changed despite the high desilication severity. The NH_3 peaks appear slightly later than those of propylene (Fig. 5c) due to re-adsorption/desorption, as previously indicated [42–45]. The NH_3-TPD and IPA-TPD results are summarized in Table 2. The Brønsted acid density estimated from the TPD measurements is in good agreement with the nominal density of HZSM-5 corresponding to a Si/Al ratio of 75 (i.e., 0.22 mmol/g). Both techniques show that the total acid density and Brønsted acid density remain largely unchanged upon desilication. A slight increase for mild desilication followed by a slight decrease with increasing desilication severity seems to be detected by both techniques, but the changes are very small.

3.1.3. Diffusivity

Fig. S1 (in Supplementary content) shows the evolution profiles resulting from sending an *n*-butane pulse through the reactor with and without a zeolite bed. The presence of the zeolite significantly changes the shape and width of the observed peak as a result of the combination of adsorption and diffusion through the zeolite bed. It is observed that, upon mild desilication, the elution peak initially shifts to longer retention time and becomes wider (compare *P* and *DS1*), but it shifts back to shorter times and becomes narrower as the degree of desilication increases (compare *DS2* and *DS4*). The apparent diffusivity derived from applying the dispersion model for deviations from plug flow to the data [47] are summarized in Table 3. Details of the fitting method are included in the Supplementary content. It is seen that the apparent diffusivity first decreases slightly (*DS1*) but then increases gradually (*DS4*). Increased diffusivities upon desilication have been previously reported [26,29]. But, at the same time, decreases in diffusivity have also been reported [30]. While increased diffusivities can be expected from enhanced mesoporosity, decreases have been ascribed to enhanced Al concentration in the desilicated zeolite that affects adsorption and may lower diffusivity.

However, the adsorption effects may not be as determinant of the overall zeolite performance as the changes in diffusion path length. For example, Gobin et al. [48] have shown that in MFI crystals (3–5 μm), the rate-determining step of the overall transport is intracrystalline diffusion. The situation seems to be the same in the present study, in which relatively large crystallite sizes have been used and very minor changes in acid density have been observed after desilication. In fact, at the larger extents of desilication (samples *DS2* to *DS4*) significant increases in apparent diffusivity are seen, and they correspond well with the increase in mesoporous volume accompanied by a shortening in the diffusion path length.

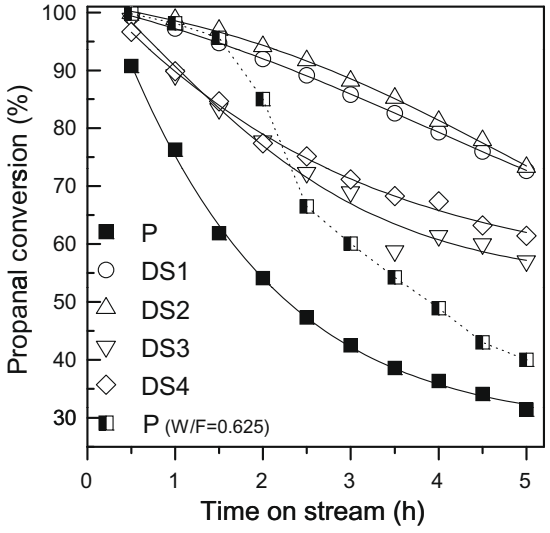

Fig. 6. Propanal conversion as a function of time on stream on parent zeolite (*P*) and desilicated (DS) zeolite samples. Reaction conditions: W/F = 0.5 h, T = 400 °C. For one run, the W/F was changed to 0.625 h (dotted line).

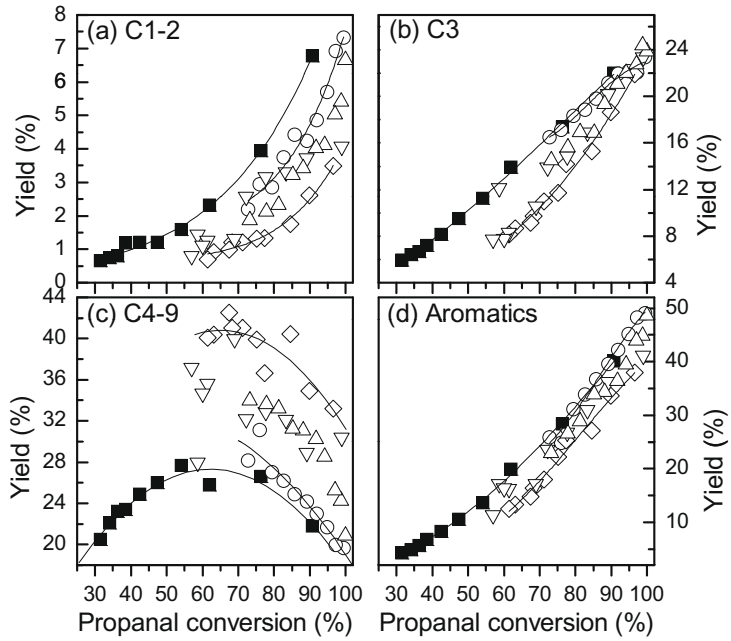

Fig. 7. Product distribution as a function of conversion, which changes with time on stream over the various zeolite samples, *P* (■); *DS1* (o); *DS2* (△); *DS3* (▽); *DS4* (◇). Reaction conditions: *W*/*F* = 0.5 h, *T* = 400 °C.

The slight decrease in apparent diffusivity for the mildly desilicated *DS1* sample might be ascribed to the increase in microporous volume combined with the minor increase in accessibility of adsorbate to the micropore structure.

3.2. Catalytic activity

3.2.1. Effect of time on stream

Fig. 6 shows the evolution of propanal conversion with time on stream. It can be seen that after a few hours under identical reaction conditions, the propanal conversion obtained on the desilicated samples is significantly higher than on the original sample *P*. The order of conversion after a few hours on stream is *DS1* ≈ *DS2* > *DS3* ≈ *DS4* > *P*. To distinguish the effects of catalyst stability from level of activity, sample *P* was run at a higher *W*/*F* (0.625 h, dotted line in Fig. 6) so for the first couple of hours the level of conversion was similar to that of *DS1*. However, after that, the conversion dropped much more rapidly than over *DS1*. Therefore, it appears that the desilicated samples exhibit not only a higher activity, but also a higher stability.

Fig. 7 shows the variation of product yields as a function of conversion for varying time on stream at constant *W*/*F*, e.g. conversion decreasing as the catalyst deactivates. A significant change in product distribution upon desilication is clearly evident. While the yield of aromatics greatly increased with conversion for all samples, an important difference is observed for the production of C4-9 alkane/alkene (mainly C5+) products compared to C3. While the light hydrocarbon fractions (C1-2 and C3) follow a similar trend to that of aromatics, that is, increasing with propanal conversion, the C4-9 alkane/alkene fraction exhibits a maximum at intermediate propanal conversions. Products in the C4-9 fraction are converted to C1-3 and aromatics as propanal conversion increases. With increasing desilication severity, the yields of C1-2, C3, and aromatics decrease while the yield of C4-9 alkane/alkene increases. Table 4 shows the product distribution for all samples at a propanal conversion of ~90%. It is evident that desilication causes a decrease in the fraction of C1-2 hydrocarbons, toluene, and *p*-xylene, but an increase in C4-9 alkane/alkene and C10+ aromatics. A noticeable difference in the product distribution observed in this study compared to studies conducted at lower temperatures is the lack of products containing oxygen. Even at the lowest conversion levels, no oxygenates other than unconverted propanal were observed in significant amounts.

3.2.2. Effect of varying space time (W/F)

The product distribution as a function of *W*/*F* was compared for the parent sample (*P*), the mildly desilicated sample (*DS1*), and the highly desilicated sample (*DS4*). Fig. 8 shows the change in propanal conversion with increasing *W*/*F*, which is higher for *DS1* and *DS4* than for *P* over the entire *W*/*F* range. As discussed later, the higher activity of *DS1* may be associated with rapid transport of propanal into the micropore channels. Fig. 9 shows the variation

Table 4
Product distribution of propanal conversion over parent and desilicated HZSM-5 with a propanal conversion of 90%.

Product yield (mol.%)	*P*	*DS1*	*DS2*	*DS3*	*DS4*	*DS4*-Si[a]
Non-aromatics						
C1-2	6.8	4.8	4.0	3.7	2.6	2.8
C3	22.0	22.0	21.0	20.2	18.6	22.1
C4-9	21.8	23.0	30.2	28.9	34.9	34.4
Aromatics						
Benzene	0.4	0.6	1.0	0.9	1.0	0.9
Toluene	8.6	8.7	6.3	6.3	5.3	5.7
C8 aromatics						
Ethylbenzene	1.8	2.0	1.4	1.4	1.2	1.3
m-Xylene	12.8	10.3	6.8	7.0	5.5	5.8
p-Xylene	1.0	2.0	2.8	2.3	2.5	3.0
o-Xylene	0.3	0.8	0.8	0.7	0.7	0.8
C9 aromatics						
Propyl-benzene	0.8	0.8	0.8	0.8	0.8	0.7
Methyl-ethyl-benzene	7.6	7.8	7.2	7.4	7.0	7.3
Trimethyl-benzene	1.6	2.7	3.3	2.2	2.1	2.4
C10+ aromatics	5.3	6.5	5.8	7.1	7.7	2.2
∑ aromatics	40.2	42.2	36.2	36.1	33.8	30.3

[a] *DS4* surface was deposited with SiO_2 to passivate the strong acid sites on the surface. Reaction conditions: *T* = 400 °C, *W*/*F* = 0.5 h.

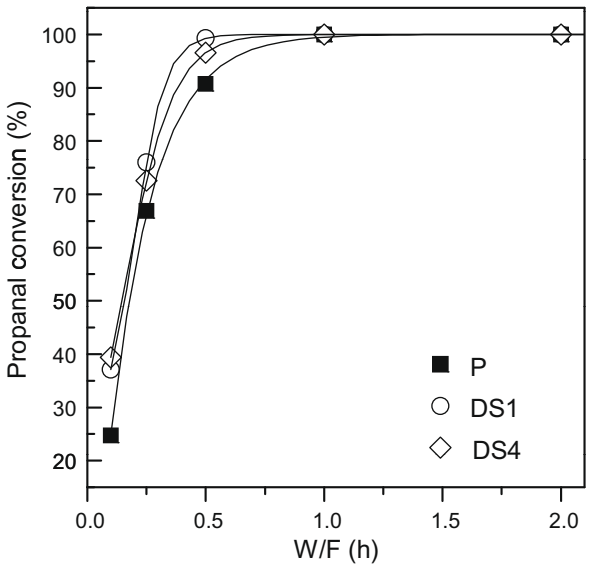

Fig. 8. Propanal conversion as a function of space time (*W*/*F*). Samples *P* (parent zeolite), mildly desilicated (*DS1*) and heavily desilicated (*DS4*). Reaction conditions: time on stream = 0.5 h, *T* = 400 °C.

of the product distribution with *W*/*F*. At low *W*/*F* (<1 h), the yields of C1-2, C3, and aromatics increase with a similar trend, while the yield of C4-9 initially increases and then decreases as this fraction is either cracked or aromatized at higher *W*/*F* when the rate of production is decreased.

The effect of desilication on product distribution is pronounced. Comparison between samples *P*, *DS1*, and *DS4* in Fig. 9 reveals that *DS1* has a higher capability for aromatization than the other two, while *DS4* shows the highest selectivity to C4-9 with the lowest extent of cracking. These differences are more clearly illustrated in Fig S2, which shows that the mildly desilicated sample *DS1* has a higher aromatics/C3 ratio, but also higher C1-2/C3 and C1-2/C4-9 ratios at higher *W*/*F*. By contrast, the more highly desilicated sample *DS4* has significantly lower aromatics/C3 ratio, but the highest C4-9/C1-2 ratio.

Fig. 10 shows the distribution of aromatic products as a function of *W*/*F*. It is observed that the yields of C7 and C8 increase with space time, while the yield of C9 initially increases and then decreases; the heavier C10+ aromatics remain at a relatively low level. Again, to better illustrate the trends, the product ratios are shown in Fig. S3. It is clear that the ratio of lighter-to-heavier aromatics increases with *W*/*F* as dealkylation of heavier products results in lighter aromatics. Interestingly, the differences in the evolution of this ratio for the three samples parallel the behavior shown in Fig. S2. That is, compared to the parent sample *P*, the extent of cracking and extent of dealkylation are significantly higher on the mildly desilicated sample *DS1* but significantly lower in the highly desilicated sample *DS4*.

3.2.3. Coke formation during reaction

Temperature Programmed Oxidation (TPO) was carried out to evaluate the amount and type of coke deposits over the zeolite after 5 h of reaction (TOS). The evolution of CO_2 (a) and H_2O (b) as a function of oxidation temperature is shown in Fig. 11. A major CO_2 peak centered at 633 °C is observed for sample *P*. The peak gradually shifts to lower temperatures as the desilication severity of the samples increases, reaching 593 °C for the most highly desilicated sample, *DS4*. In parallel, a smaller peak centered at 432 °C develops gradually. The gradual growth of this peak coincides with the growth of a H_2O peak at the same temperature that, as shown in Fig. 11b, grows with increasing desilication severity. The other H_2O evolution peak (576 °C) is dominant for the original *P* sample, but it gradually reduces in intensity as the peak at 434 °C grows. The dissimilar trends of the CO_2 and H_2O curves indicate that there are at least two types of coke in the zeolites, one richer in hydrogen that oxidizes at lower temperatures and the other, more hydrogen-deficient that oxidizes at higher temperatures. The hydrogen-rich carbonaceous deposits can be ascribed to a pool of alkylated aromatics and/or heavy condensation products trapped in the zeolite mesopores and micropores [49]. In contrast, the hydrogen-deficient deposits are described as polyaromatic or pseudo-graphitic coke [49]. The significant shifts to lower temperatures of the CO_2 peak upon desilication are accompanied by an increase in H_2O evolution, indicating an increase in the fraction of hydrogen-rich coke with increasing desilication severity. As shown in Table 5, while sample *DS1* exhibited after reaction slightly less coke than sample *P*, the other desilicated samples showed somewhat higher amounts. Despite forming comparable or even higher amounts of coke, the desilicated samples are able to maintain higher conver-

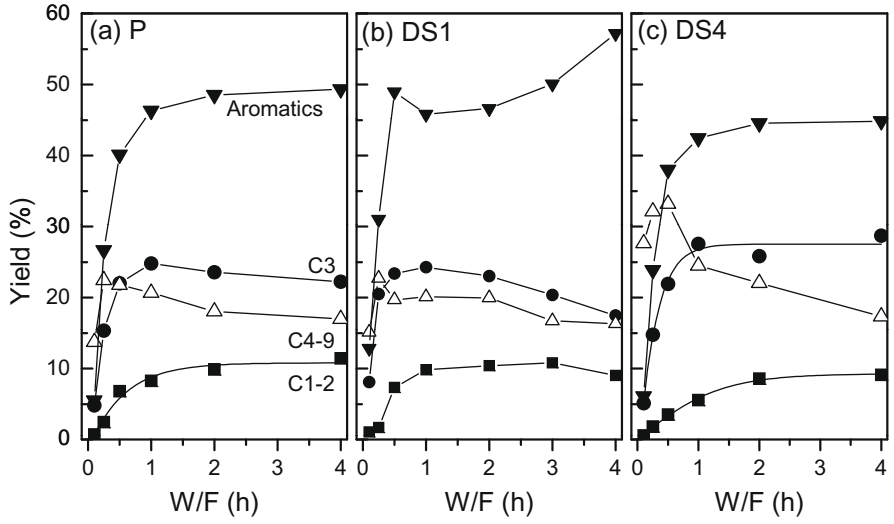

Fig. 9. Product distribution as a function of *W*/*F*. C1-2 (■); C3 (●); C4-9 (△); aromatics (▼). Samples *P* (a); *DS1* (b), and *DS4* (c). Reaction conditions: time on stream = 0.5 h, *T* = 400 °C.

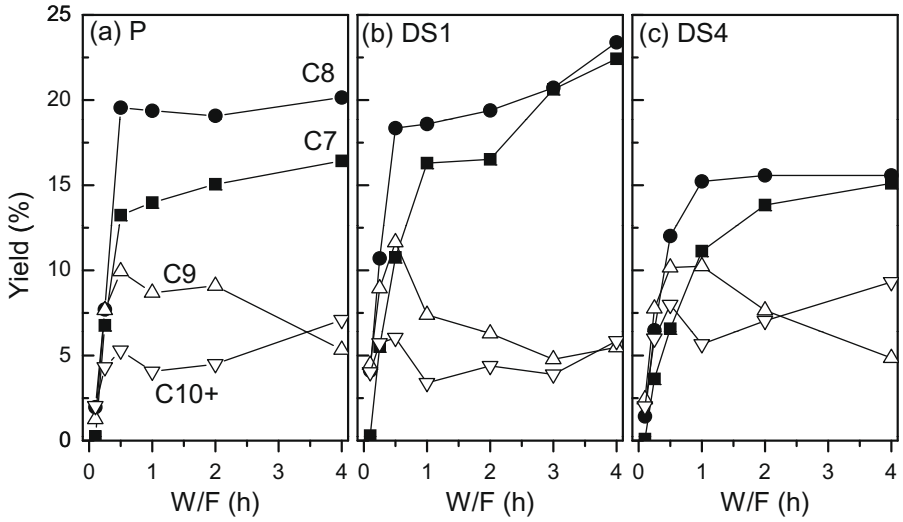

Fig. 10. Variation of distribution of aromatic products with *W*/*F* for sample *P* (a), *DS1* (b), and *DS4* (c). Aromatics of C7 (■); C8 (●); C9 (△); C10+ (▽). Reaction conditions: time on stream = 0.5 h, *T* = 400 °C.

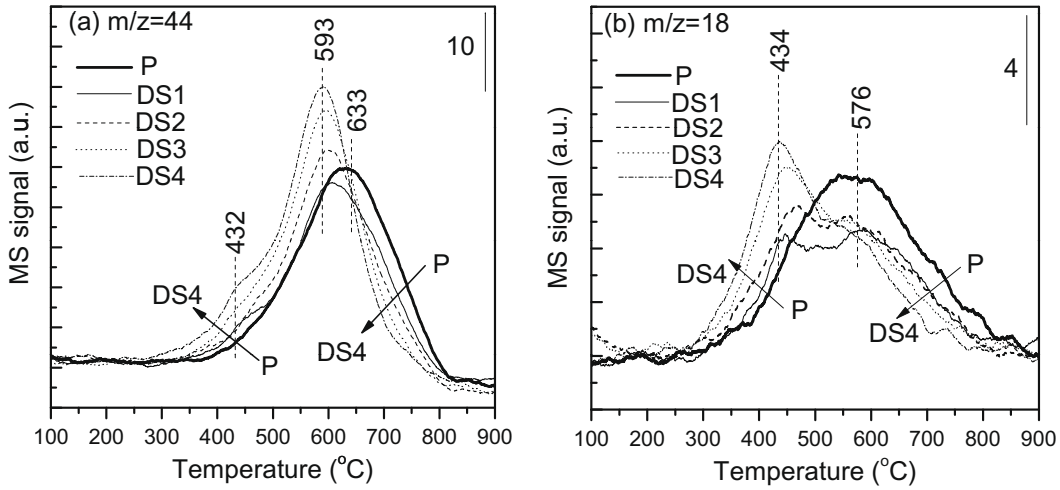

Fig. 11. Carbon dioxide (a) and water (b) evolution profiles during temperature programmed oxidation of carbonaceous deposits on spent catalysts for parent (*P*) and desilicated (DS) zeolite samples. Reaction conditions: *W*/*F* = 0.5 h, time on stream = 5 h, *T* = 400 °C.

Table 5
Carbon content on spent catalysts for parent (*P*) and desilicated (DS) zeolite samples. Reaction conditions: *T* = 400 °C, *W*/*F* = 0.5 h, time on stream = 5 h.

Sample	*P*	*DS1*	*DS2*	*DS3*	*DS4*
Carbon (wt.%)	5.6	4.3	5.7	6.3	6.4

sion for hours, implying that the hydrogen-rich coke has less influence in blocking the accessibility to the micropores. That is, they are probably deposited in the mesopore structure.

4. Discussion

Acid-catalyzed condensation reactions of aldehydes and ketones can produce a large variety of compounds that depend on the reaction conditions and catalysts. Acetone, which has a similar C=O bond as in propanal, has been extensively studied for both, aldol condensation [50] and conversion to aromatics [12,18–20,51–53]. It has been proposed that conversion of acetone over acid zeolites can consecutively produce dimer and trimer via aldol condensation. At relatively low temperatures (~250 °C), the trimer easily converts to mesitylene (1,3,5-trimethyl benzene) via cyclization and dehydration [18–20,51,52]. It has been proposed that, at higher temperatures (>300 °C), the α,β-unsaturated ketone formed by dehydration of the dimer undergoes hydrolysis to form isobutene, and then this isobutene converts to aromatics [18–20,51,52]. Since propanal is even more reactive than acetone [19], it is expected that over highly acidic catalysts such as H-ZSM-5, it can undergo similar condensation and cyclization pathways to form aromatics. Scheme 1 summarizes the major possible reaction paths that propanal can undergo under the conditions of this study. Self-condensation of propanal produces first a dehydrated dimer (2-methyl pentenal) and then a trimer (2,4-dimethyl 2,4-diene heptenal) that is essentially the building block for the observed products. Neither the dimer nor the trimer is observed in the products at the high temperatures of this study (400 °C) due to their high reactivity. Further studies by our research group at lower temperatures provide evidence for the formation of the dimer and trimer species [54]. In those studies, we have seen that the trimer can directly cyclize to form a C9 aromatic (mesitylene) through internal self-condensation (ring closure) and dehydration.

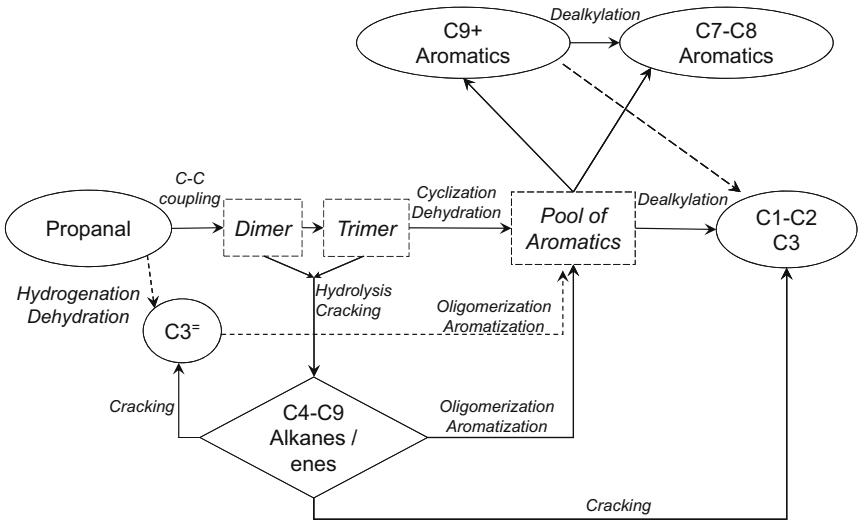

Scheme 1. Acid-catalyzed major pathways in the high-temperature conversion of propanal.

At the same time, both the dimer and trimer can also hydrolyze or decarbonylate forming the observed C4-9 alkanes/alkenes. These medium-size alkanes/alkenes undergo further oligomerization, cyclization, and aromatization to form the observed alkyl-aromatics through the conventional hydrocarbon aromatization pathway, in line with the observed initial increase and subsequent decrease in C4-9 alkane/alkene concentration. The alkyl-aromatics formed from both internal condensation of trimer and alkene oligomerization/aromatization may act as a hydrocarbon pool in the zeolites that can lead to coke or further condensation with the propanal feed, as previously proposed [55]. The alkyl-aromatics (C9+) have a low diffusivity (long residence time) inside the micropores of HZSM-5. Thus, further reactions of alkyl transfer, dealkylation, and cracking inside the micropores result in the formation of C7-8 aromatics, C1-2 light gases, and C3 (mainly propylene).

The detailed characterization study conducted on the samples has demonstrated that as the severity of desilication increases, the degree of mesoporosity developed in the ZSM-5 crystals increases significantly. The resulting variation in the meso/micropore ratio has a considerable effect on catalyst activity, stability, and selectivity. The study shows that the development of mesopores has no significant influence on the density of Brønsted acid sites. That is, the extent of propanal adsorption and reaction intermediates should not be significantly altered by desilication. Therefore, the important changes in product distribution observed across the catalyst series must be explained in terms of the alteration of the meso/microstructure balance.

To interpret the changes in product distribution upon desilication, one must take into account that the reduction in diffusion path length shortens the residence time of the intermediates (i.e. oxygenated dimers, trimers, and C4-9 alkenes) in the micropores, where aromatization takes place. As a result, the overall conversion to aromatics decreases in the highly desilicated samples. The reduction in microporosity and concomitant enhanced diffusion also lead to less cracking, as seen in the decreased yield of C1-2. It should be noted that it is the large reduction in C1-2 yield that results in the large increase in the C3/C1-2 ratio with increasing desilication severity (see Table 4). At the same time, dealkylation is reduced in this catalyst, which results in decreased C7-8 aromatics and increased C9-10+ aromatics (see Figs. 10 and S3 and Table 4).

The analysis of the xylene distribution provides further insight on the effects of the micro/mesoporous structure on selectivity. That is, while at 400 °C, the equilibrium distribution of xylenes is about *p*:*m*:*o* = 1.0:2.2:1.0 [18], the observed distribution is the 12.8:1:0.3 for sample *P* and gradually changes to 2.2:1:0.28 for sample *DS4* (Table 4). That is, *p*-xylene is strongly favored on the parent zeolite as a result of the well-known shape selective transformation inside the micropores [56]. Increasing desilication severity leads to shorter diffusion path length due to mesopore formation, which in turn results in shorter residence time for xylene isomers inside the micropores, causing a decrease in the extent of *o*-, and *m*-xylenes transformation to *p*-xylene.

It is well known that active sites for aromatization in HZSM-5 are the Brønsted acid sites. However, as shown in Fig. 12, the yield of aromatics at 90% conversion over the different samples does not correlate well with the density of Brønsted acid sites (A_B), but it seems to correlate with the micropore volume of the samples. That is, it appears that only the Brønsted acid sites inside the micropores are responsible for aromatization. Increasing the desilication severity leads to higher amounts of Brønsted acid sites outside the micropores and on the surface of the mesopores generated by desilication. This conversion is possibly accompanied by formation of small amounts of Lewis sites, as suggested by recent IR studies that used a bulky probe molecule, like collidine [46,28]. In order to differentiate the effects that the mesoporous/microporous balance may have on product distribution from those caused

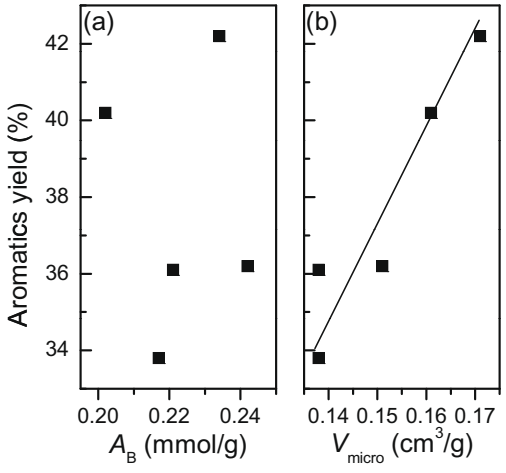

Fig. 12. Correlation of aromatics yield with (a) Brønsted acid density, and (b) micropore volume.

by changes in the location of the acid sites, additional experiments were performed on the severely desilicated sample (*DS4*) further passivated by SiO_2 deposition [57] (see details in Supplementary content). It is expected that passivation selectively deactivates the strong acid sites located on the outer and mesoporous surface without greatly affecting those sites located in the microporous structure. As shown in the last column of Table 4, the SiO_2-passivated sample (*DS4*-Si) shows slightly lower C4-9 yield than *DS4*, but still much higher than *P*. As shown in Fig. S4, the same behavior is observed over a wide propanal conversion range. That is, the generation of acid sites on the outer and mesoporous surface cannot be responsible for the significantly higher C4-9 selectivity exhibited by the severely desilicated samples.

The catalyst stability seems to be improved by desilication. However, only the mildly desilicated sample (*DS1*) shows a moderate reduction in the rate of coke formation. By contrast, the rest of the desilicated samples show a modest increase in the amount of coke formation with increasing desilication severity. Based on the earlier discussion, one can conclude that both the changes in diffusion path length and the addition of mesoporous surface acid sites (both B and L acid sites) may influence the amount and type of coke formation. Shortening the diffusion length can reduce carbon deposition because the larger molecules generated in the zeolite can leave the micropores effectively, before further transformation into hydrogen-deficient species. At the same time, increasing the amounts of strong acid sites in the mesopore can enhance adsorption of heavy molecules. This kind of coke located in the mesopores can be hydrogen-rich, as observed experimentally.

The slightly lower amount of coke formed over the *DS1* sample is related to the combination of two effects, a shortened diffusion path length and a lower amount of mesoporous surface acid sites. However, as the severity of the desilication increases (*DS2* to *DS4*), higher amounts of condensation (hydrogen-rich) coke are observed.

5. Conclusions

Desilication of ZSM-5 using alkaline solutions with varying strengths of basicity, temperature, and time leads to the development of structures with varying mesoporosity. XRD, SEM, and N_2 adsorption confirms increasing generation of mesoporosity with increasing desilication severity. NH_3-TPD and IPA-TPD provide evidence that desilication causes little variation in Brønsted acidity, accompanied by formation of Lewis acid sites in the severely desilicated sample. The pulse response studies of the various catalysts using *n*-butane as a tracer show that mild desilication favors molecular penetration into the micropores. Increasing desilication severity results not only in shortened diffusion path lengths in the micropores but also in easier transport through the mesoporous structure, which results in a more rapid removal of the tracer from the catalyst bed.

Propanal conversion over HZSM-5 produces C7–C10+ aromatics, C4-9 alkanes/alkenes, C3 (mainly propylene), and C1-2 cracking products. Mesopore development improves the stability of the catalyst for propanal conversion as well as coke tolerance. The mildly desilicated sample has the best conversion stability and lowest coke formation. Increasing the extent of desilication gradually reduces the aromatization capability and cracking reactions due to a reduction in microporosity and a shortening of the diffusion path length.

Acknowledgments

This work has been supported, in part, by the NSF EPSCoR award EPS 0814361 and the Department of Energy (DoE Grant GO88064). Support from the Oklahoma Bioenergy Center is greatly appreciated. The authors thank Prof. C.J. Liu and Ms. Y. Liu in Tianjin University for their kind help with the N_2 adsorption measurements.

Appendix A. Supplementary material

Supplementary data associated with this article can be found, in the online version, at doi:10.1016/j.jcat.2010.02.004.

References

[1] J.N. Chheda, G.W. Huber, J.A. Dumesic, Angew. Chem. Int. Ed. 46 (2007) 7164.
[2] G.W. Huber, S. Iborra, A. Corma, Chem. Rev. 106 (2006) 4044.
[3] D.A. Simonetti, J.A. Dumesic, ChemSusChem 1 (2008) 725.
[4] S. Czernik, A.V. Bridgwater, Energy Fuel 18 (2004) 590.
[5] D. Mohan, C.U.P. Pittman Jr., P.H. Steele, Energy Fuel 20 (2006) 848.
[6] M.A. Peralta, T. Sooknoi, T. Danuthai, D.E. Resasco, J. Mol. Catal. A 312 (2009) 78.
[7] T.R. Carlson, G.A. Tompsett, W.C. Conner, G.W. Huber, Top. Catal. 52 (2009) 241.
[8] M. Olazar, R. Aguado, J. Bilbao, A. Barona, AIChE J. 46 (2000) 1025.
[9] P. Chantal, S. Kaliaguine, J.L. Grandmaison, A. Mahay, Appl. Catal. 10 (1984) 317.
[10] P.T. Williams, P.A. Horne, J. Anal. Appl. Pyrol. 31 (1995) 39.
[11] A.G. Gayubo, A.T. Aguayo, A. Atutxa, R. Aguado, J. Bilbao, Ind. Eng. Chem. Res. 43 (2004) 2610.
[12] A.G. Gayubo, A.T. Aguayo, A. Atutxa, R. Aguado, M. Olazar, J. Bilbao, Ind. Eng. Chem. Res. 43 (2004) 2619.
[13] J.D. Adjaye, N.N. Bakhshi, Biomass Bioenergy 8 (1995) 131.
[14] J.D. Adjaye, N.N. Bakhshi, Fuel Process. Technol. 45 (1995) 185.
[15] A. Corma, G.W. Huber, L. Sauvanaud, P. O'Connor, J. Catal. 257 (2008) 163.
[16] B. Katryniok, S. Paul, M. Capron, F. Dumeignil, ChemSusChem 2 (2009) 719.
[17] N. Gyorffy, Z. Paal, J. Mol. Catal. A 295 (2008) 24.
[18] C.D. Chang, A.J. Silvestri, J. Catal. 47 (1977) 249.
[19] J. Fuhse, F. Bandermann, Chem. Eng. Technol. 10 (1987) 323.
[20] G.J. Hutchings, P. Johnston, D.F. Lee, A. Warwick, C.D. Williams, M. Wilkinson, J. Catal. 147 (1994) 177.
[21] R.M. Dessau, E.W. Valyocsik, N.H. Goeke, Zeolites 12 (1992) 776.
[22] R.L. Van Mao, S.Y. Xiao, A. Ramsaran, J.H. Yao, J. Mater. Chem. 4 (1994) 605.
[23] A. Cizmek, B. Suboti, R. Aiello, F. Crea, A. Nastro, C. Tuoto, Microporous Mater. 4 (1995) 159.
[24] M. Ogura, S. Shinomiya, J. Tateno, Y. Nara, E. Kikuchi, M. Matsukata, Chem. Lett. (2000) 882.
[25] J.C. Groen, J.C. Jensen, J.A. Moulijn, J. Pérez-Ramírez, J. Phys. Chem. B 108 (2004) 13062.
[26] J.C. Groen, W.D. Zhu, S. Brouwer, S.J. Huynink, F. Kapteijn, J.A. Moulijn, J. Pérez-Ramírez, J. Am. Chem. Soc. 129 (2007) 355.
[27] C.H. Christensen, K. Johannsen, E. Törnqvist, I. Schmidt, H. Topsøe, C.H. Christensen, Catal. Today 128 (2007) 117.
[28] F. Thibault-Starzyk, I. Stan, S. Abelló, A. Bonilla, K. Thomas, C. Fernandez, J.-P. Gilson, J. Pérez-Ramírez, J. Catal. 264 (2009) 11.
[29] L. Zhao, B.J. Shen, J.S. Gao, C.M. Xu, J. Catal. 258 (2008) 228.
[30] M. Ogura, S. Shinomiya, J. Tateno, Y. Nara, M. Nomura, E. Kikuchi, M. Matsukata, Appl. Catal. A 219 (2001) 33.
[31] C.S. Mei, P.Y. Wen, Z.C. Liu, H.X. Liu, Y.D. Wang, W.M. Yang, Z.K. Xie, W.M. Hua, Z. Gao, J. Catal. 258 (2008) 243.
[32] S. Gopalakrishnan, A. Zampieri, W. Schwieger, J. Catal. 260 (2008) 193.
[33] M. Bjørgen, F. Joensen, M.S. Holm, U. Olsbye, K.-P. Lillerud, S. Svelle, Appl. Catal. A 345 (2008) 43.
[34] L.L. Su, L. Liu, J.Q. Zhuang, H.X. Wang, Y.G. Li, W.J. Shen, Y.D. Xu, X.H. Bao, Catal. Lett. 91 (2003) 155.
[35] Y.N. Li, S.L. Liu, Z.K. Zhang, S.J. Xie, X.X. Zhu, L.Y. Xu, Appl. Catal. A 338 (2008) 100.
[36] S. Brunauer, P.H. Emmet, E. Teller, J. Am. Chem. Soc. 60 (1938) 309.
[37] B.C. Lippens, J.H. de Boer, J. Catal. 4 (1965) 319.
[38] E.P. Barrett, L.G. Joyner, P.P. Halenda, J. Am. Chem. Soc. 73 (1951) 373.
[39] J.C. Groen, L.A.A. Peffer, J.A. Moulijn, J. Pérez-Ramírez, Colloid Surf. A 241 (2004) 53.
[40] D. Ohayon, R.L. Van Mao, D. Ciaravino, H. Hazel, A. Cochennec, N. Rolland, Appl. Catal. A 217 (2001) 241.
[41] J.C. Groen, L.A.A. Peffer, J.A. Moulijn, J. Pérez-Ramírez, Chem. Eur. J. 11 (2005) 4983.
[42] W.E. Fameth, R.J. Gorte, Chem. Rev. 95 (1995) 615.
[43] T.J. Gricus Korke, R.J. Gorte, G.T. Kokotailo, W.E. Farneth, J. Catal. 115 (1989) 265.
[44] T. Sooknoi, T. Danuthai, L.L. Lobban, R.G. Mallinson, D.E. Resasco, J. Catal. 258 (2008) 199.
[45] C. Pereira, R.J. Gorte, Appl. Catal. 90 (1992) 145.
[46] M.S. Holm, S. Svelle, F. Joensen, P. Beato, C.H. Christensen, S. Bordiga, M. Bjørgen, Appl. Catal. A 356 (2009) 23.
[47] O. Levenspiel, Chemical Reaction Engineering, third ed., Wiley, 1999.

[48] O.C. Gobin, S.J. Reitmeier, A. Jentys, J.A. Lercher, J. Phys. Chem. C 119 (2009) 20435.
[49] L. Palumbo, F. Bonino, P. Beato, M. Bjørgen, A. Zecchina, S. Bordiga, J. Phys. Chem. C 112 (2008) 9710.
[50] G.S. Salvapati, K.V. Ramanamurty, M. Janardanarao, J. Mol. Catal. 54 (1989) 9.
[51] P. Dejaifve, J.C. Védrine, V. Bolis, E.G. Derouane, J. Catal. 63 (1980) 331.
[52] S. Deane, K. Wilshier, R. Western, T. Mole, D. Seddon, J. Catal. 88 (1984) 499.
[53] A.I. Biaglow, J. Sepa, R.J. Gorte, D. White, J. Catal. 154 (1995) 208.
[54] T.Q. Hoang, X.L. Zhu, T. Sooknoi, D.E. Resasco, R.G. Mallinson, J. Catal. (2010), doi:10.1016/j.jcat.2010.01.017.
[55] M.J. Climent, A. Corma, H. Garcia, J. Primo, J. Catal. 130 (1991) 138.
[56] J. Wei, J. Catal. 76 (1982) 433.
[57] P.J. Kunkeler, D. Moeskops, H. van Bekkum, Microporous Mater. 11 (1997) 313.